COMPREHENSIVE CHARACTERIZATION OF MOTION OF A HELICAL STRUCTURE DUE TO FLOW INDUCED VIBRATION

P.L. Harmon and W.R. Marcum
Department of Nuclear Engineering & Radiation Health Physics, Oregon State University
3451 Jefferson Way Corvallis, OR USA
harmonp@onid.oregonstate.edu; wade.marcum@oregonstate.edu

ABSTRACT

Mechanical vibrations compromise the integrity of key components of thermal power plants. Without careful design, strong resonances during steady state operation can wear these components to the point of failure, leading to an unsafe situation that may force a plant to shut down. The purpose of this research is to further the understanding of the vibrations induced in a helical structure, or coil, subject to steady coolant flow. A helical coil steam generator, such as that found in most integral pressurized water reactors, appears to eliminate many flow-induced vibration concerns when compared to traditional steam generators; however this has yet to be clearly demonstrated experimentally. The objective of this work is to develop a method of characterizing the motion of a helical coil in an annulus subject to external cross-flow of water. This is accomplished by observing the motion of a helical coil mounted to an inner opaque cylinder through an outer glass tube using a high speed video camera. A mirrored image-pair is used to observe this structure from two perspectives simultaneously, allowing for three-dimensional characterization of the coil motion. The experimental facility is described in detail. The method of identifying specific points on the coil from images and mapping them to the coil location using the law of refraction is described. A MATLAB code conducts temporal measurement of the coil motion. An uncertainty analysis of the coil position measurement is conducted based on geometry and refractive index which can be readily applied to measurements obtained using this method.

KEYWORDS
Helix, Flow Induced Vibrations, Index of Refraction, Fluid Structure Interactions

1 INTRODUCTION

Heat exchangers and emission control systems have high length to width aspect ratios which make them susceptible to mechanical vibrations. They are designed to maximize heat transfer and generation, reduce footprint or increase particulate sequestration. Flow passes these elements at a rapid rate, causing periodic pressure changes that induce vortices and structural oscillations. Without careful design, strong resonances during steady state operation wear these components to the point of failure, leading to hazardous conditions and potential shutdowns.

Examples of power plant components sensitive to mechanical vibrations are boilers, condensers, and steam generators. Their heat exchanging elements include hundreds of long tubes bundled together inside pressure vessels. These are often inaccessible to repair after installation without prohibitive cost. Also, emissions control systems in coal-fired plants, such as electro-static precipitators and selective catalytic reduction systems, have large parallel-plate arrangements that are regularly vibrated to remove particulate build-up. Finally, vibration or bowing of precisely spaced cylinders or parallel plates in a reactor core increases high temperature peaks which affect the determination of plant power rating.

For example, the pressurized water reactor (PWR) at San Onofre, California is being decommissioned due to leakage of primary coolant through ruptured tubes in its steam generator. Changes in the steam generator design as well as manufacturing and handling issues caused the steam generator tubes to vibrate excessively during steady state operation. This led to fretting of the pipes and their rapid deterioration. The PWR at San Onofre was forced to close permanently and is presently being decommissioned, incurring heavy expenses to its parent company, the manufacturer of the failed components and the rate-payers in the area. This event underscores the need for careful consideration of flow-induced vibrations of high aspect ratio heat exchanging elements relevant to current power plant design as a necessary feature for safe and continuous plant function.

Problems with steam generator vibrations in nuclear power plants are not new. The Enrico Fermi atomic power plant, which operated from 1963 to 1972, was a fast breeder reactor operating next to Lake Erie [1]. As a sodium-cooled reactor, the plant had a complex design for its steam generator. Designers had to account for the possible reaction of sodium with water while providing an efficient transfer of heat. Flow of sodium at the steam generator inlet induced excessive vibrations in its serpentine tubes. Wearing between the tubes and their restraints allowed water to leak into the sodium coolant, incurring extensive damage. The general causes of the wear were identified as insufficient restraint of tubes near the inlets of the sodium coolant, where the flow velocity was high and the failures observed, and as insufficient baffling of these inlets to reduce flow velocity [2].

Sandusky et. al. [3] noted that steam generators for most integral reactor designs, which have a helical coil geometry, are less susceptible to flow induced vibrations than traditional designs. However, this has not been verified experimentally, and further study is needed to confirm this assumption. Study in this area is complicated by a number of factors. The characteristic natural frequency of a coil changes dramatically when immersed in a dense liquid. Resonance is also affected when the coil is in close proximity to a solid surface, as when the coil windings are spaced less than their width apart or near a cylindrical wall. Failure is difficult to predict partly because the structural vibration of helical coils under steady fluid flow is currently not well understood.

A large body of similar work on the vibration and fluidelastic instability of tube arrays has been conducted on bundles of cylinders [4], [5], [6]. However, a smaller number assess the characteristics of a helical coil geometry. A number of numerical and analytical models have been proposed referencing historical datasets [7], [8], [9]. Experimental tests have been conducted on spring oscillations in a tube with simplifications applicable for the phenomena being addressed. These included allowing the spring to rest fully on an inner cylinder [10] or sectoring the helical coil bundle into an array of curved tubes [11]. A thorough study by Blevins [12] provides a wealth of information on the flow induced vibrations of air flow past a large helically coiled superheater. However, constraints of this experiment, such as large and stiff tube coils, restricted observations to those of stable motion.

Structural dynamic characterization is typically conducted using sensors mounted to the structure directly [13]. This method works well for large structures in dry systems, but the mass of the sensor encumbers small structures and operation in liquid typically degrades sensor performance. Sensors are typically placed inside of immersed hollow tubes [14], but the tube inner diameter has to be sufficiently large to mount the sensor. A non-invasive approach to analyzing position measurement for smaller tube or wire coils is more appealing. General methods have been developed for analyzing motion using imaging techniques based on direct observation [15]. If it is necessary to look at a motion occurring behind a surface, the wall is usually made flat [16], [17] or carefully modified to physically remove the effects of refraction [18]. However, using ray tracing techniques outlined by Lowe and Kutt [19], optical refraction through a clear outer cylinder can be calculated and the position of points on a coil measured. The uncertainty due to this refraction can be quantified following a method similar to Patil and Liburdy [20] in their characterization of refractive index mismatch.

The purpose of this research is to further the understanding of the vibrations induced in a helical structure, or coil, subject to steady coolant flow. A helical coil with a major diameter concentric to an inner and outer cylinder is a proposed geometry to reduce flow-induced vibration in a heat exchanger element. In this configuration the outer coolant readily flows over the coil windings, promoting heat transfer. The thinnest fluid channels are formed in the gaps between each loop of the coil and between the coil and the cylinder walls. With supports constraining motion only at its ends, the flexibility of the coil's central windings will allow for observable motion from flow induced vibrations.

To accomplish this, an experimental facility with a helical coil in an annulus is constructed and a method for characterizing its motion when subject to external cross-flow of water is developed. Controlled vibration experiments are conducted by incrementally varying flow rates. The facility is designed with instruments to measure pressure drop over the coil and locate coil edge positions. A method is developed to obtain motion frequency over a range of flow rates. The effect of uncertainty on the measurement of edge positions is studied and comparisons are made to existing literature.

2 MATERIALS AND METHODS

The design of this facility includes considering the natural frequency of the coil, the rate of fluid flow, and the structure affixing the coil in place. The fluid velocity is adjustable to allow the frequencies of fluid oscillations and structural natural frequency to be matched. To observe motion due to instability, flow must reach a 'critical velocity'. The motion should be observable and the geometry controlled to reduce uncertainties in structures affecting position measurements.

To achieve significant convective heat transfer, heat exchangers typically have high flow rates. Their characteristic size is large and the viscosity of the heated fluid low, leading to high Reynolds numbers that can exist over the range of $10^6 - 10^8$. This flow regime is difficult to achieve in a small scale experiment. To these ends, rather than matching the Reynolds number of a typical heat exchanger, this facility is designed to create the flow conditions necessary to induce structural vibrations in the test coil due to vortex shedding and fluidelastic instability. To accomplish this, the Reynolds number of the flow with respect to the coil wire diameter must be sufficient to create regular vortices and a uniform turbulent flow in the annulus, and the maximum flow velocity must be greater than the critical threshold for fluidelastic instability.

To approximate the geometry of a helical coil heat exchanger, the coil is centered between an inner and outer cylinder as shown in Figure 1. While heat exchangers typically have numerous banks of coiled tubes, this facility simplifies the observation by exciting a single coiled wire. To estimate the fundamental frequency of a wire coil, the critical frequency of a compression spring is applied as described by Budynas and Nisbett [21]. This is derived from its total strain energy due to a vertical force on the coil winding. The critical frequency of a compression coil between parallel plates is given to be,

$$f_1 = \frac{1}{2}\left(\frac{\mathrm{k}}{m}\right)^{\frac{1}{2}}. \tag{1}$$

Here f_1 is the critical frequency due to surging between parallel plates, k is the structure's stiffness, and m is the structure's mass. This can be further detailed by substituting relations for coil stiffness and mass to solve for frequency in terms of wire coil dimensions,

$$f_1 = \frac{1}{2\pi N_a D^2}\left(\frac{Gd^2}{\rho_c\left(1+\frac{d^2}{2D^2}\right)}\right)^{\frac{1}{2}} \tag{2}$$

where N_a is the number of active coils, D is the major diameter of the helix, d is the wire diameter, G is the shear modulus of the material, and ρ_c is the added density of the wire material and displaced fluid. This density approximates the effect of added mass of the natural frequency of a cylinder. As the wire diameter becomes much smaller than the major helix diameter, the frequency becomes directly proportional to wire diameter and inversely proportional to the number of active coils and the square of the major helix diameter. In order to visually observe oscillations, this frequency would ideally be minimized, making a wide helix with multiple coils and a small wire diameter preferable.

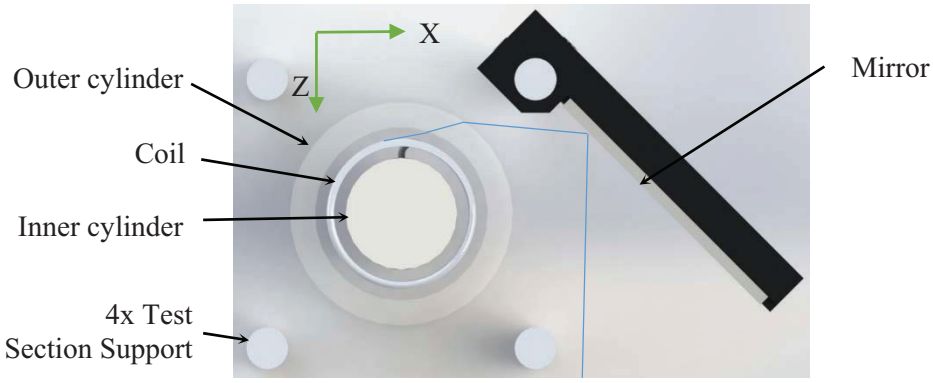

Figure 1. Test element horizontal cross section

The frequency of vortex shedding past a bluff body is described by the Strouhal number, St. For a circular cylinder, the Strouhal number has been shown to maintain a nearly constant value over a wide range of Reynolds numbers. Fluid velocity, U, is directly related to the frequency of the vortex shedding in this range,

$$f = \frac{StU}{d}. \tag{3}$$

When this frequency begins to coincide with the structure's natural frequency, the 'lock-in' phenomenon occurs increasing the amplitude of motion at a single frequency.

As discussed by Jiang Nai-bin et. al. [22], fluidelastic instability in arrays of tubes causes the amplitude of oscillations to grow rapidly when the flow exceeds a critical velocity. This velocity can be estimated using Connors' bound for critical velocity as described by Yang [23] for an array of cylinders,

$$V_c = \beta f_n \left(\frac{2\pi\zeta_n m_t}{\rho_f} \right)^{\frac{1}{2}} \tag{4}$$

where V_c is the critical flow velocity, β is Connors' Constant assumed to have a value of 4.0, ζ_n is the damping ratio with an assumed value of 0.015 for tubes submerged in water, m_t is the total mass per unit length of the wire, and ρ_f is the fluid density. In this case, the coil is not an array, but only has a single cylinder which is wrapped into an in-line array. Instability is only seen when multiple structures are present; it is not clear if this coil geometry will display instability or not. The Connors' Constant, based on average trends of historical experimental datasets, is used.

Pressure drop across the coil was estimated using drag coefficients of cylinders. This determines the sensitivity required for pressure measurements. The first full turn is treated as a straight circular cylinder in cross-flow from Munson [24] and subsequent turns as cylinders in a square array from Koch and Ladd [4]. The resulting pressure drop across the coil is estimated as 0.016 psid across the coil at 1.2 gpm flow, which increases for higher flow rates. This value was used to select the lower bound of the combined

accuracy of pressure sensors. Pressure drop across the overall test section is estimated using form losses from entrance and exit of fluid into and out of the test section and major losses along the annulus are quantified using area change form losses and friction factors from Munson [24]. Entrance length of flow before the test element is about twenty hydraulic diameters to allow the profile to stabilize in the annulus.

Refraction of light through the sight glass and fluid causes magnification of the coil image. This affects both the straight and mirrored views. Values for the indices of refraction used to quantify this effect which are taken from Hecht [25] and Corning Inc. [26] are presented along with focal lengths in Table I. Uncertainties in indices were not given so are assumed to the based on the least significant digit. Using the test element centered two dimensional ray tracing technique described by Low and Kutt [19], the observed radius of the tangent outer coil edge with respect to the helix central axis, R_P, is determined by,

$$R_P = L\frac{n_0}{n_f}\sin(\Omega), \tag{5}$$

$$R'_P = L_M\frac{n_o}{n_f}\sin(\Omega') \tag{6}$$

and

$$y = \left(L_f\left(\frac{n_o}{n_f}-1\right)+L_w\left(\frac{n_0}{n_w}-1\right)+L\right)\Phi. \tag{7}$$

Here, L is the physical distance from the base of the camera lens to the axis of the helical coil, n_0 is the index of refraction for air, n_f the index for water, and Ω the angle between a line from the axis of the helix to the camera lens and the ray incident on the lens as shown in Figure 2. Increasing the physical distance between the coil axis and the camera reduces the difference in magnification between the direct and mirrored views. The angle can be quantified by counting the pixels between features in a camera image and comparing this value to the pixel count from an edge that subtends a known angle. The assumption of the helix concentric to the outer cylinder and the ray tangent to a point on this helix allowed for significant simplification of this equation.

Table I. Test section optical parameters

Parameter	Value
Air Index	1.000277 ± 0.000001
Water Index	1.333 ± 0.001
Borosilicate Glass (Pyrex) Index	1.474 ± 0.004
Direct View *L* [in]	2.353 ± 0.001
Mirrored View *L* [in]	24.3 ± 0.50
Length of Calibration Edge [in]	27.2 ± 0.75
Calibration Edge *L* [in]	3.95 ± 0.005

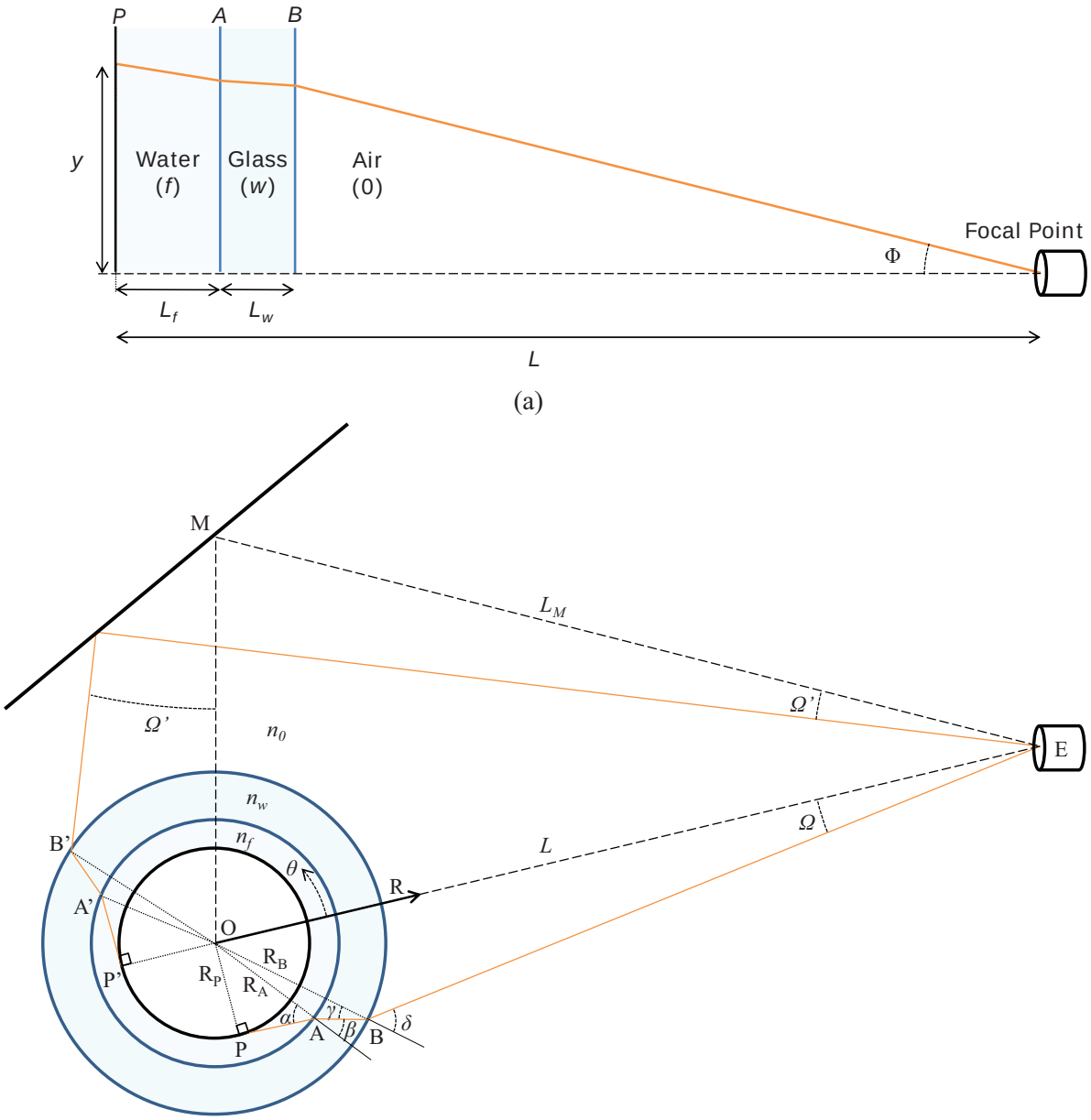

Figure 2. (a) vertical and (b) horizontal ray trace from camera to coil

The Camera-Observed and Instrumented Loop (COIL) Facility uses a high speed camera and pressure transducers to analyze cross-flow induced vibrations of a test element over a range of flow rates. A model of the facility is presented in Figure 3. As shown in Figure 4, a clear borosilicate glass cylinder allows for visual access to the element under analysis and an angled mirror provides a simultaneous second view for three-dimensional reconstruction. The high speed camera, a Phantom model VR 0411, has a maximum acquisition rate of 14 kHz and a pixel resolution ranging from 200 to 500 pixels per inch depending on camera position. The test element is a malleable 1100 Aluminum wire wound into a helical coil by use of a printed form. It is attached to an inner cylinder by bending the coil ends through two holes perpendicular to the cylinder axis. Piping connects the test section to a fluid reservoir with flow provided by a one-third horsepower pump. Control valves on two parallel Key rotameters give manual control of flow rate from 0.4 to 12.0 gpm. Omega pressure transducers with piezo-resistive technology and a range

up to 15 psig are mounted before and after the test section to give gage and differential pressure across the test section within 0.015 psi accuracy overall. A front surface mirror covered in highly reflective aluminum provides a simultaneous second view. Water temperature is monitored by a K-type thermocouple. The liquid is room temperature local water. A National Instruments compact DAQ platform acquires pressure and temperature data. A bypass loop allows for low flow velocities without damaging the centrifugal pump.

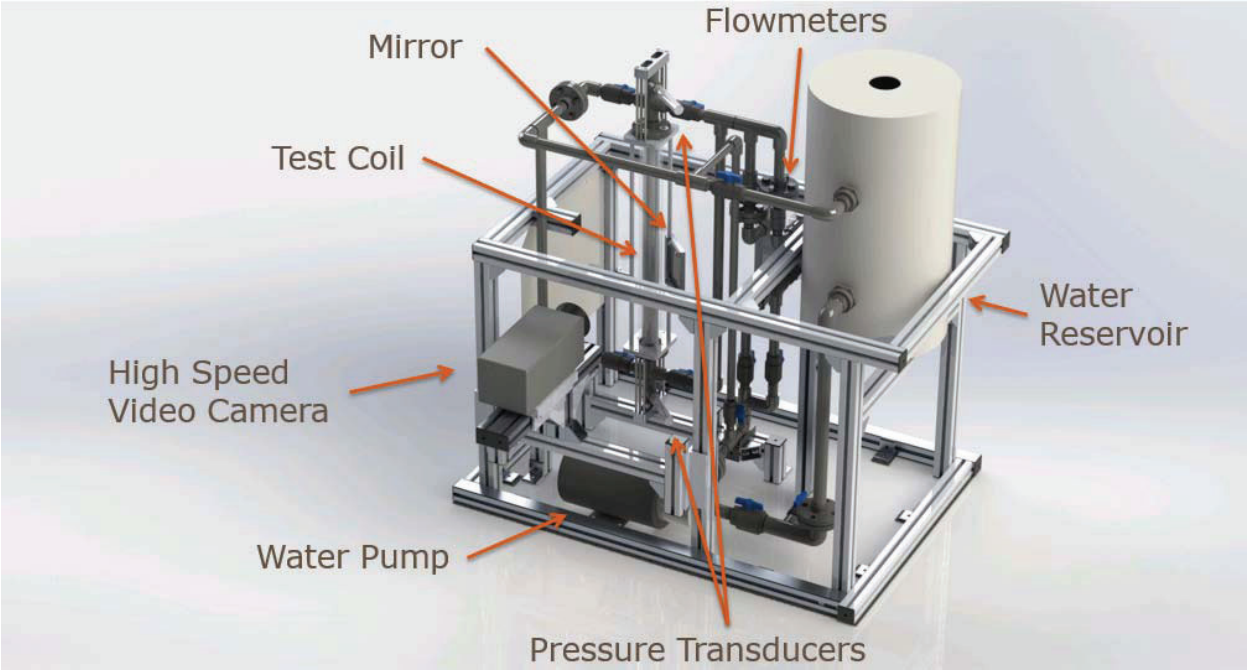

Figure 3. COIL facility

Each captured image has two views of the coil, a direct and a reflected view. The magnification effect is slightly reduced in the reflected view because of the longer path taken by a reflected ray. The direct view captures horizontal (X) and vertical (Y) position, while the mirrored view captures depth (Z) and vertical (Y) position as shown in Figure 4. Since the pair of views are in the same image, they are captured simultaneously without the added uncertainty of time difference that accompanies multiple camera approaches.

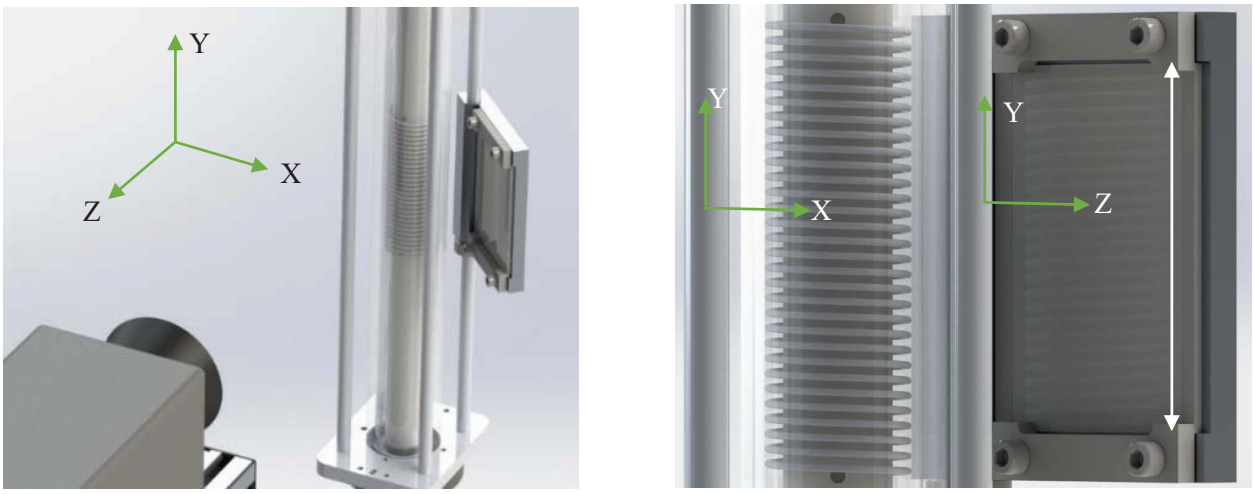

Figure 4. Test section with camera (left) and camera view (right)

From the side, a circular cylindrical coil appears as a semicircle where a turn loops back on itself. The center of this semicircle is a close estimate to the center of the wire. To identify this semi-circle, an image is first converted to binary to allow for clear contrast between coil edge and background. The region of interest about where a coil edge should appear is first manually identified in first image pair. Since the amplitude of edge motion is relatively small, the average and standard deviations of position locations are calculated and used along with the largest observed semicircle diameter and a small buffer to establish regions of interest for further images in a sequence. A circle recognition function in MATLAB obtains circle centers and radii from these regions using a two-stage Hough method. This method uses a 'voting' technique where pixels are given a greater probability of being a circle if they are surrounded equidistantly by gradients in grayscale intensity that point toward a single location [27]. While conditions of poor lighting or low contrast can lead to incorrect identification of edge centers, this technique works well when the curve of the edge is sufficiently visible and the contrast between the edge and its background is uniform.

To calibrate an image sequence, a reference length of a machined edge, as indicated by the arrow in Figure 4, and the physical distance of the lens to this edge are identified. Rays from tangent edges of the coil to the lens focal point are mapped as shown in Figure 2. Using equation (5), pixel values are scaled to position dimensions. For magnification, the points from the direct and mirrored views are assumed to lie on the XY and YZ planes through the helix centerline, respectively. The edges are analyzed vertically from top to bottom with the edges appearing in the mirrored image determining the section of coil to be modeled. The coils are close enough together that the difference in magnification between the mirrored and straight views makes identifying the order of the coil edges somewhat difficult requiring verification of ordering after pixel values have been converted to position values.

Using the dimensions presented in Table II, predicted flow rates are calculated as 3.8 gpm for lock-in and 6.0 gpm for instability. The calculated frequency of the coil is 20.0 Hz and the pressure drop across the coil is calculated at 0.098 psid at 3.0 gpm. The flow rate through the test section was manually set by rotameter. After flow had reached a steady state, images were acquired using the Phantom Cine Viewer software at a 200 Hz rate over a one second period. This reduced rate allowed sufficient time to collect enough light in each image to resolve coil edges. The images were analyzed using a MATLAB script which identified coil centers in each image and converted raw pixel information to spatial position accounting for refraction and focal length. A fast Fourier transform was conducted for each edge over the sequence of images to identify the frequency of motion in the X and Y directions described in Figure 4.

Table II. Geometry of test section

Parameter	Value
Mean Coil Diameter [in]	1.50 ± 0.10
Wire Diameter [in]	0.0808 ± 0.005
Coil Pitch [in]	0.1616 ± 0.050
Number of Turns	30 ± 0.1
Annulus Inner Diameter [in]	1.161 ± 0.003
Annulus Outer Diameter [in]	1.823 ± 0.001
Entrance region length [in]	12.0 ± 0.003

3 RESULTS

Figure 5 outlines the process utilized to reconstruct the positional state of the helical coil for each camera image collected during the experimental program. Figure 6 presents both a raw image and a processed binary image with coil edge circles programmatically located and outlined in blue.

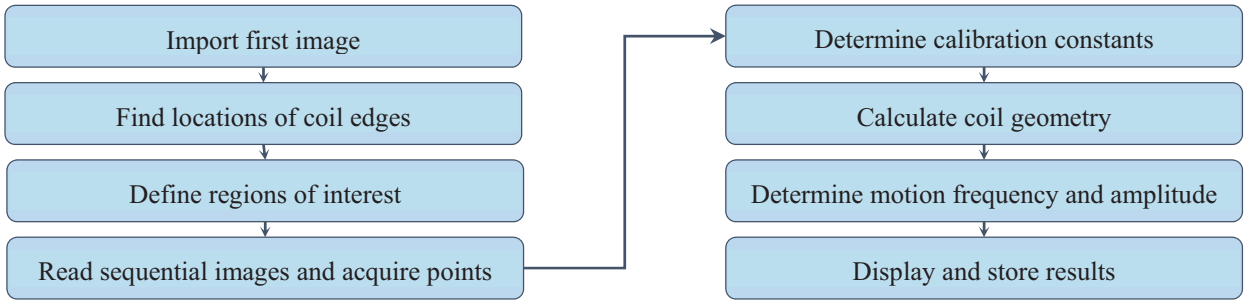

Figure 5. Flowchart of Matlab program for determining coil positions

Isometric, front and side views of the coil geometry pictured in Figure 6 are shown in Figure 7. A set of points selected for position and frequency analysis are identified with red asterisks. Measured point locations from all coil edges are shown with blue dots in Figure 7. The dashed line is an interpolation between the quadrant measured points using MATLAB's spline function.

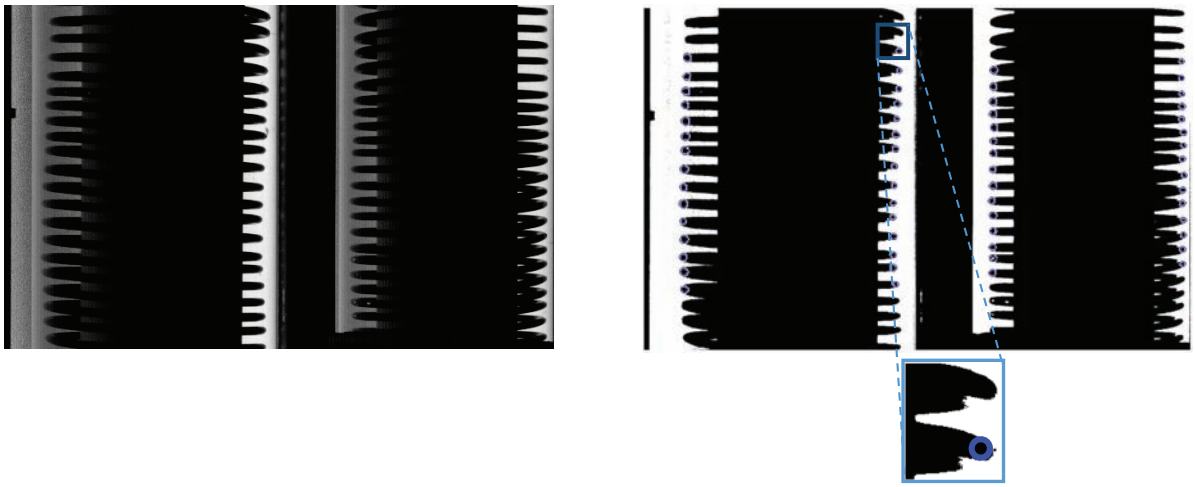

Figure 6. Raw image of coil (left), binary image with edge center locations mapped (right)

The position of a single point is tracked in the XZ plane for 1.0, 2.0 and 3.0 gpm respectively in Figure 8. The normalized spectral plots in Figure 9 and Figure 10 display the X and Y frequencies respectively of the identified edges from one second image sequence periods over the tested flow rates. In this case, the measured lock-in frequencies at a 3.0 gpm flowrate were identified within 1.0 Hz of 28.0 Hz in the X direction and within 1.2 Hz of 28.8 Hz in the Y direction for the five points analyzed.

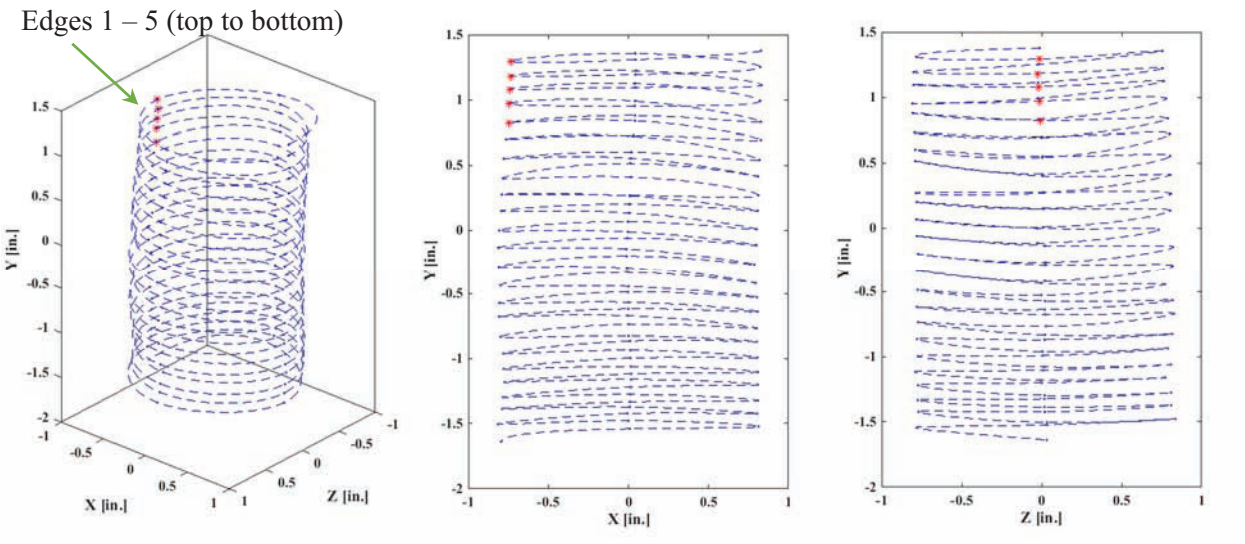

Figure 7. Reconstructed coil geometry isometric (left), front (center), and side (right)

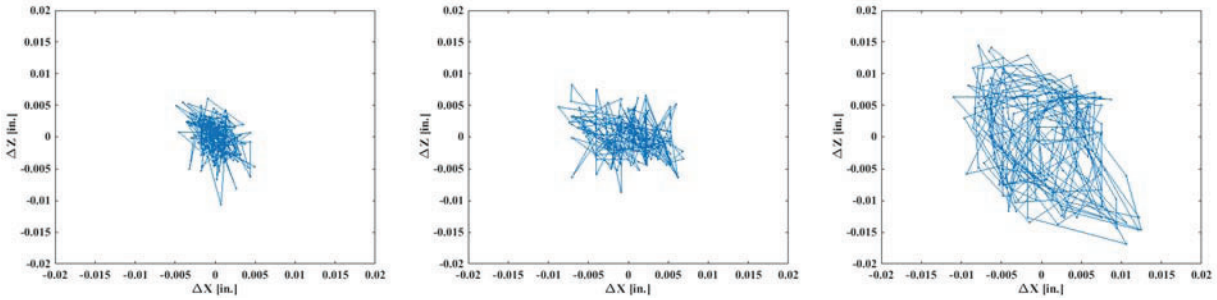

Figure 8. Single point X and Z motion at 1.0 (left), 2.0 (center), and 3.0 (right) gpm

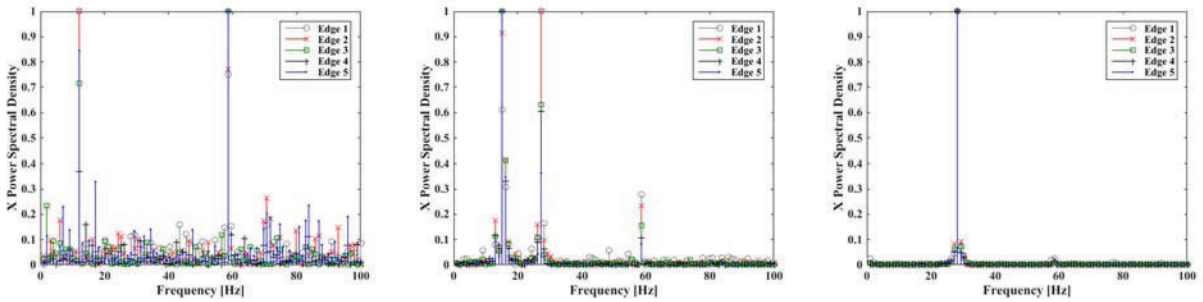

Figure 9. Normalized spectral plots in X direction at 1.0 (left), 2.0 (center), and 3.0 (right) gpm

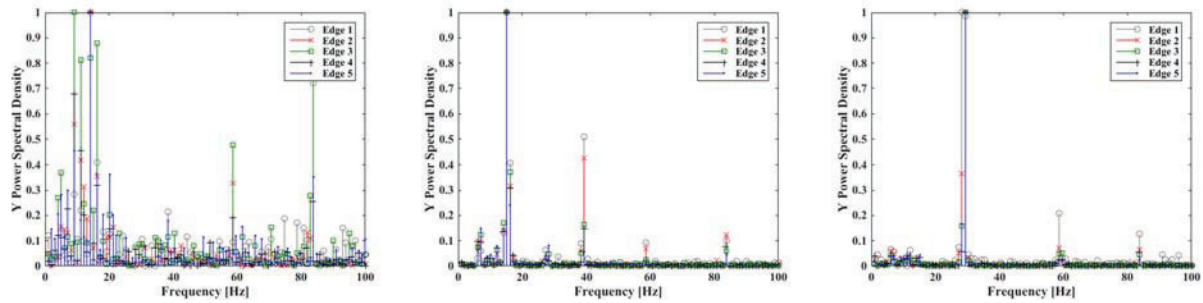

Figure 10. Normalized spectral plots in Y direction at 1.0 (left), 2.0 (center) and 3.0 (right) gpm

4 DISCUSSION

As can be seen in the reconstructed coil geometry in Figure 7, there is some over prediction of the curve radius at the ends. This region proves to be the most difficult region to reconstruct since there are fewer points to use for interpolation. This interpolation scheme is most successful where it has a sufficient number of surrounding points. The incrementally reduced pitch at the base of the coil due to drag of the downward flow is observable in the reconstructed geometry.

Use of MATLAB's circle finding function has a number of benefits and drawbacks, as can be observed in Figure 6. It improves analysis time and resolution with programmatic identification and interpolation between pixels compared to manual selection which is slow and restricted to pixel location. However, shadows in the background or on the coil can cause it to select optical aberrations as coil centers as seen in the reflected image at the top right and midway down the left side. More uniform lighting about the structure and surface treatment to prevent reflections on the coil would improve contrast in these areas.

As shown in Figure 8 through Figure 10, the amplitude of motion observed in the 1.0 gpm flow test was small and the measured frequencies fairly random. As flow increased, cohesive frequencies became more pronounced as the period of vortex shedding approached that of the structural vibration. Higher modes at multiples of 29 Hz are also observed when compared against the predicted natural frequency of the coil during the design process (20 Hz). The 3.0 gpm flow appears to match the vortex shedding with the structural natural frequency, causing a single frequency to dominate. There is a range of flow over which lock-in may occur; observing this phenomenon at a lower flow rate than predicted is not unusual. This demonstrates that the method is capable of capturing physical effects of flow induced vibrations on a helical coil. Greater resolution of motion frequency can be achieved by increasing the period of image capture at the cost of increased computation time.

For approximating vertical magnification, the same magnification method was used as for the horizontal magnification. While this is a good approximation for small angles, the rays take a slightly longer path through the sight glass for large angles which affects the measured position.

Factors contributing to position uncertainty include coil-to-sight glass concentricity, component dimensions, and refraction indices. The concentricity of the inner cylinder with respect to the outer sight glass has some variability based on the structures locating these two components. This was controlled to within ± 0.018 inches based on tolerances of the connecting parts. This added to the uncertainty in mounting the coil concentrically to the inner cylinder, on the order of half the diameter of the wire, leads to an axial offset between the coil and sight glass. Also, measurement uncertainties of the dimensions of the sight glass, focal lengths, and mean distance between the mirror and coil center could lead to error in the position measurement. The effect of these uncertainties can be quantified by,

$$\sigma_{\Delta R_P} = \frac{n_0}{n_f} L\left(\left(\cos\left(\Omega_2\right)\right)^2 {\sigma_{\Omega_2}}^2 + \left(\cos\left(\Omega_1\right)\right)^2 {\sigma_{\Omega_1}}^2\right)^{1/2} \tag{8}$$

and

$$\sigma_{\Delta y} = \left(\left(L_f\left(\frac{n_0}{n_f}-1\right)+L_w\left(\frac{n_0}{n_w}-1\right)+L\right)^2 \sigma_{\Phi 2}^2 + \left(L_f\left(\frac{n_0}{n_f}-1\right)+L_w\left(\frac{n_0}{n_w}-1\right)+L\right)^2 \sigma_{\Phi 1}^2\right)^{1/2}. \tag{9}$$

Given the values for uncertainty in Table I and Table II, the overall position uncertainty would then be ± 0.003 inches in X and Z directions for each point. The greatest contribution to this uncertainty is in mounting the coil, which could be improved by a mechanism to rigidly affix it in place. The axial offset, *AO*, affects the measured position in these directions since the outer diameter of the clear outer cylinder

cannot be identified in the image. The Y direction uncertainty is about ± 0.0039 inches since it is not affected by axial offset.

Low flow rates were used in these tests to reduce the amplitude of motion of the coil and test the facility and method by observing the stable approach to lock-in. At higher flow velocities, Fujita [10] noted that coil motion was limited by the coil striking the surrounding container. This amplitude of motion was not required for position observation and allowed for simple identification of regions of interest where coil edges might be. By conducting tests in a controlled manner, improvements to the facility and method could be identified and implemented before proceeding to explore more complex phenomena.

5 CONCLUSIONS

A series of tests were conducted to evaluate the method of characterizing the shape of a helical coil subject to external flow. An experimental facility was designed and constructed to accomplish this using a high speed video camera. Sequential images were acquired and processed using feature recognition functions in a MATLAB script. The pixel values were then converted to position and the three dimensional shape reconstructed. Position over time was analyzed to obtain the frequency of motion in two directions for select points. Motion frequency increased with increasing flowrate, and the effect of lock-in was clearly seen. Uncertainty of position was quantified based on geometry and refractive indices. The capability to measure edge positions and reconstruct coil geometry is demonstrated along with motion tracking and frequency analysis over multiple images.

6 ACKNOWLEDGMENTS

We appreciated the help of Musa Moussaoui and Suyang Liu in constructing the facility. Insights by Aaron Weiss and Warren Jones in our discussions on the design and manufacture of numerous components helped improve this project.

7 REFERENCES

1. Commission, U.S.N.R. *Fermi, Unit 1*. 2015.
2. Shin, Y.S. and M.W. Wambsganss, *Flow-induced vibration in LMFBR steam generators: A state-of-the-art review.* Nuclear Engineering and Design, 1977. **40**(2): p. 235-284.
3. Sandusky, D., et al., *Assessment of Materials Issues for Light-Water Small Modular Reactors*. 2013, National Technical Information Service: Alexandria, VA.
4. Koch, D.L. and A.J.C. Ladd, *Moderate Reynolds Number Flows through Periodic and Random Arrays of Aligned Cylinders.* Journal of Fluid Mechanics, 1997. **349**: p. 31-66.
5. Weaver, D.S., et al., *Flow-Induced Vibrations in Power and Process Plant Components-Progress and Prospects.* Journal of Pressure Vessel Technology, 2000. **122**(3): p. 339-348.
6. Ibrahim, R.A., *Mechanics of Pipes Conveying FLuids-Part II: Applications and Fluidelastic Problems.* Journal of Pressure Vessel Technology, 2011. **133**(2): p. 1 - 30.
7. Shifang, S. and D. Xingzhong. *Finite Element Method for Natural Vibration Analysis of Helical Tube Array*. in *Transactions of the International Conference on Structural Mechanics in Reactor Technology*. 1993. Stuttgart, Germany.
8. Jo, J.C. and M.J. Jhung, *Flow-induced vibration and fretting-wear predictions of steam generator helical tubes.* Nuclear Engineering and Design, 2008. **238**(4): p. 890-903.
9. Xu, H., M. Mallet, and T. Liszkai. *Turbulent Buffeting of Helical Coil Steam Generator Tubes*. in *ASME 2014 Pressure Vessels & Piping Conference*. 2014. Anaheim, California, USA: ASME.
10. Fujita, K., et al., *Study on the Axial-Flow-Induced Vibration of Coil Springs.* Journal of Fluids and Structures, 1993. **7**(6): p. 689-705.

11. Chen, S.S., J.A. Jendrzejczyk, and M.W. Wambsganss, *Tube Vibration in a Half-Scale Sector Model of a Helical Tube Steam Generator.* Journal of Sound and Vibration, 1983. **91**(4): p. 539-569.
12. Blevins, R.D. *Turbulence-Induced Vibration of Heat Exchanger Tubes in Cross Flow*. in *American Society of Mechanical Engineers Pressure Vessels and Piping Conference*. 1994. Minneapolis, MN.
13. Clemens, R., et al. *Structural Dynamic Characterization of Small-Scale Multipurpose Payloads Using Conventional and Fiber Optic Sensors*. in *SPIE Smart Structures and Materials+ Nondestructive Evaluation and Health Monitoring*. 2013. San Diego, CA.
14. Lin, T.-k. and M.-h. Yu, *An experimental study on the cross-flow vibration of a flexible cylinder in cylinder arrays.* Experimental Thermal and Fluid Science, 2005. **29**(4): p. 523-536.
15. Chang, C.C. and Y.F. Ji, *Flexible Videogrammetric Technique for Three-Dimensional Structural Vibration Measurement.* Journal of Engineering Mechanics, 2007. **133**(6): p. 656-664.
16. Amini, N. and Y.A. Hassan, *Measurements of jet flows impinging into a channel containing a rod bundle using dynamic PIV.* International Journal of Heat and Mass Transfer, 2009. **52**(23-24): p. 5479-5495.
17. Yoo, J., C.E. Estrada-Perez, and Y.A. Hassan, *A proper observation and characterization of wall nucleation phenomena in a forced convective boiling system.* International Journal of Heat and Mass Transfer, 2014. **76**: p. 568-584.
18. de Witt, B.J., H. Coronado-Diaz, and R.J. Hugo, *Optical contouring of an acrylic surface for non-intrusive diagnostics in pipe-flow investigations.* Experiments in Fluids, 2008. **45**(1): p. 95-109.
19. Lowe, M.L. and P.H. Kutt, *Refraction Through Cylindrical Tubes.* Experiments in Fluids, 1992. **13**(5): p. 315-320.
20. Patil, V.A. and J.A. Liburdy, *Optical Measurement Uncertainties due to Refractive Index Mismatch for Flow in a Porous Media.* Experiments in Fluids, 2012. **53**(5): p. 1453-1468.
21. Budynas, R.G. and J.K. Nisbett, *Shigley's Mechanical Engineering Design, 8th Edition*. 2008, New York: McGraw-Hill.
22. Nai-bin, J., et al., *An unsteady model for fluidelastic instability in an array of flexible tubes in two-phase cross-flow.* Nuclear Engineering and Design, 2015. **285**: p. 58-64.
23. Au-Yang, M.K., *Flow-Induced Vibration of Power and Process Plant Components*. 2001, New York: ASME.
24. Munson, B.R., D.F. Young, and T.H. Okiishi, *Fundamentals of Fluid Mechanics*. 2006, Wiley. p. 770.
25. Hecht, E. and A. Zajac, *Optics 4th (International) Edition*. 2002: Addison Wesley.
26. Corning, I. *Properties of PYREX®, PYREXPLUS® and Low Actinic PYREX Code 7740 Glasses*. [cited 2015 February 27th]; http://www.quartz.com/pxprop.pdf].
27. Yuen, H.K., et al., *Comparative-study of Hough transform methods for circle finding.* Image and Vision Computing, 1990. **8**(1): p. 71-77.